NASA TECHNICAL MEMORANDUM

NASA TM X-71555

NASA TM X-71555
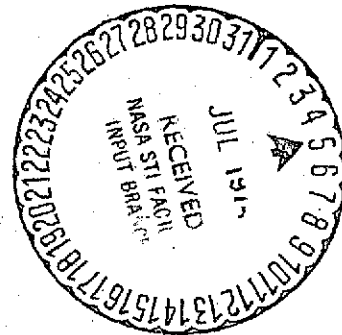
GUIDING CENTER MODEL TO INTERPRET NEUTRAL PARTICLE ANALYZER RESULTS

by G. W. Englert, J. J. Reinmann,
and M. R. Lauver
Lewis Research Center
Cleveland, Ohio

GUIDING CENTER MODEL TO INTERPRET NEUTRAL PARTICLE ANALYZER RESULTS

by G. W. Englert, J. J. Reinmann, and M. R. Lauver

Lewis Research Center

ABSTRACT

The theoretical model accounts for drift and cyclotron components of ion motion in a partially ionized plasma. Density and velocity distributions are systematically prescribed. The flux into the neutral particle analyzer (NPA) from this plasma is determined by summing over all charge exchange neutrals in phase space which are directed into apertures. Calculation of the process is continued through the NPA using appropriate cross section data to obtain analyzer output distributions. Theoretical results were compared with NPA measurements on four plasma heating devices having radial electric, E, fields and axial magnetic, B, fields. Drift velocity, in the azimuthal direction, is identified with E/B. Especially detailed data, obtained by sweeping the line of sight of the apertures across the plasma of the NASA Lewis HIP-1 burnout device, are presented. Selection of randomized cyclotron velocity distributions about mean azimuthal drift yield energy distributions which compare well with experiment. Use of data obtained with a bending magnet on the NPA showed that separation between energy distribution curves of various mass species correlate well with a drift divided by mean cyclotron energy parameter of the theory. Use of the guiding center model in conjunction with NPA scans across the plasma aid in estimates of ion density and E field variation with plasma radius.

INTRODUCTION

Determination of ion motion in a plasma from diagnosis of the escaping charge exchange neutrals is made difficult by the many processes involved. Not all of the particles admitted into the apertures of a neutral particle analyzer (fig. 1) influence the output signal. Only those which are suitably charged after passing through a stripping cell and which have a resulting energy, within a small spread, are able to reach the output detector. This band of energy is dependent on beam resolution and the setting of the electrostatic energy selector. Relating the motion of such terminal subgroups of particles back to the characteristics of the total ensemble of ions in the plasma involves unwieldy kinetic descriptions in phase space. Simply the selection and determination of the many concomitant multivalued roots in such an inverse type of problem can be quite tedious.

As an alternate approach, an attempt is made to model the essential features of the ion motion in the plasma. A guiding center model is hypothesized for the crossed E and B field type of heating device of interest herein. Such a forward method of solution also simplifies cal-

culation of the processes inside the NPA. Comparison of these results with experimentally determined NPA output can be used to evaluate, modify, and extend the plasma model.

The guiding center model gives results which agree with experimental data from four different plasma heating devices. This model and its evaluation are discussed herein.

PLASMA MODEL

The plasma is assumed to be axisymmetric and have a radially inward directed electric field, E, normal to the axis. The magnetic field (flux density) B, is assumed to be in the axial direction and uniform in a plane of diagnostics normal to the axis. In figure 2(a) the crossed field velocity, v_c, of a guiding center drifts clockwise about the axis of the plasma while the ion cyclotron velocity, v_{cy}, is directed counterclockwise about its guiding center. The small change of direction which a heavy particle undergoes during a charge exchange event, as well as the small time interval of interaction for the event to occur are assumed negligible. Thus in the analysis, for a particle to enter the aperture it is necessary that the vector sum of the ion drift and cyclotron velocities be directed toward the aperture at the time of the charge exchange event. From figure 2(a)

$$v_{cy}^2 = v_a^2 + v_c^2 + 2v_a v_c \sin \theta \qquad (1)$$

Here $v_a^2 = 2\varepsilon/m$ where ε is the energy of the entering neutrals which is set by the NPA. In general, $\vec{v}_c$ is dependent on the guiding center location, $\vec{r}_c$, which is displaced from the ion location by the cyclotron radius, $\vec{r}_{cy}$. From figure 2(a) and some trigonometric manipulation*

$$r_c \sin \theta = y \mp r_{cy} \sqrt{1 - (v_c \cos \theta / v_{cy})^2}$$

and using equation (1) this becomes

$$r_c \sin \theta = y \mp r_{cy}(v_a + v_c \sin \theta)/v_{cy} \qquad (2)$$

_____

*From figure 2(a)

$$r_c \sin \theta = y - r_{cy} \sin(\theta + \beta),$$

where $\theta + \beta$ is the angle that $\vec{r}_{cy}$ makes with the positive x axis. By law of sines and relation between inverse trigonometric functions

$$\theta + \beta = \cos^{-1}(v_c \cos \theta / v_{cy})$$

$$= \sin^{-1}\left[\pm \sqrt{1 - (v_c \cos \theta / v_{cy})^2}\right].$$

Here the plus sign corresponds to the case where the x component of $\vec{v}_{cy}$ is directed away from the aperture. This second solution is possible only in the lower half plane. The ions corresponding to this sign have a guiding center region nearer to the axis than those identified with the minus sign.

The magnitude of the cyclotron velocity is considered to be distributed about some mean value. For full randomization of this constituent there exists a cyclotron temperature, T_{cy}. The sizes of the domain of $\vec{r}_c$, shown by the shaded area on figure 2(a), are thus due to the spread in v_{cy} as well as to the aperture height.

The number of particles entering the apertures per unit time is equal to that of the various species which in turn can be expressed as

$$\dot{N}_a = \ell \iiint \sigma_{ch} v_a n_i(r_c) n_n(r_c) f_v(\vec{v}) r_c \, dr_c \, d\theta \, d\vec{v} \tag{3}$$

Integration is over all coordinate (r_c, θ) and three-dimensional velocity space, $\vec{v}$, from which contributions can be made. It is assumed that the velocity distribution can be broken into components parallel and perpendicular to the plasma axis.

Since the apertures have finite width, ℓ, in the axial direction, there is a dependence of N_a on $v_{||}$. For a randomized distribution of $v_{||}$,

$$f_{||}(v_{||}) = \sqrt{a}/(2e^{av_{||}^2})$$

where the constant, a, can be identified as $m/2kT_{||}$ if so desired. The contribution of $v_{||}$ to equation (3) is

$$(\sqrt{a}/2) \int_{-v_a \tan \alpha}^{v_a \tan \alpha} e^{-av_{||}^2} \, dv_{||} = (\sqrt{\pi}/2) \mathrm{erf}(\sqrt{a} \, v_a \tan \alpha)$$

$$\approx \sqrt{a} \, v_a \tan \alpha \tag{4}$$

The quantity $\tan \alpha$ is a geometrical constant as shown in figure 2(b) and the final approximation is good for small α.

At any specific location in the plasma, cyclotron velocity can vary whereas drift velocity is fixed. Thus

$$f_\perp(\vec{v}_\perp)dv_\perp = f_\perp(\vec{v}_{cy} + \vec{v}_c)d\vec{v}_{cy}$$

$$= f'_{cy}(\vec{v}_{cy})d\vec{v}_{cy}$$

$$= (1/4)v_{cy} \sin \phi \, f_{cy}(v_{cy})dv_{cy} \, d\phi$$

where ϕ is azimuthal angle and noting that f'_{cy} is isotropic in $\vec{v}_{cy}$ space. Assuming a fully randomized distribution of the magnitude of $\vec{v}_{cy}$

$$f_{cy} = (m/4kT_{cy})e^{-mv_{cy}^2/2kT_{cy}} \tag{5}$$

Substituting equation (4) and (5) into (3), integrating over ϕ, utilizing (1), and converting from velocity to energy space gives

$$\dot{N}_a = C \int_0^\infty \int_{\theta_1}^{\theta_2} \int_{r_{c,1}(\theta)/r_D}^{r_{c,2}(\theta)/r_D} \sigma_{ch} n_i(r_c/r_D) n_n(r_c/r_D)$$

$$\times \exp - \left(\mathcal{E} + v_c^2 + 2v_c\sqrt{\mathcal{E}} \sin \theta\right)\mathcal{E}(1 + v_c \sin \theta/\sqrt{\mathcal{E}})(r_c/r_D)d(r_c/r_D)d\theta \, d\mathcal{E}$$

where

$$\mathcal{E} = mv_a^2/2kT_{cy} = \varepsilon/kT_{cy}$$

$$C = \ell\sqrt{a} \, r_D^2 \, \text{tn} \, \alpha \, kT_{cy}/2m$$

Velocity and radial distance have been made dimensionless by arbitrarily dividing by $(2kT_{cy}/m)^{1/2}$ and ion diffusion radius, r_D, respectively.

The electrostatic plates of the NPA select small ranges, $\Delta\varepsilon/2$ about ε so that at the NPA output

$$\frac{\Delta\dot{N}}{\Delta\mathcal{E}} \approx \frac{d\dot{N}}{d\mathcal{E}} = C\mathcal{A}\mathcal{E}\sigma_{ch} \int_{\theta_1}^{\theta_2} \int_{r_{c,1}(\theta)/r_D}^{r_{c,2}(\theta)/r_D} n_i(r_c/r_D) n_n(r_c/r_D)$$

$$\times \exp - \left(\mathcal{E} + v_c^2 + 2v_c\sqrt{\mathcal{E}} \sin \theta\right)(1 + v_c \sin \theta/\sqrt{\mathcal{E}})(r_c/r_D)d(r_c/r_D)d\theta \tag{6}$$

where $\mathcal{A}$ is the fractional ionization of the neutrals as a result of the

stripping cell, $\mathcal{Q}$ is a factor (proportional to ϵ) accounting for the beam resolution, and κ accounts for the dependence of the output detector on the energy of the impinging particles.

Equation (6) can be numerically integrated for arbitrary density, drift, and temperature distributions. It is expedient, however, to first hypothesize various elementary reference models in order to determine the sensitivity of results to the large number of free variables and to make preliminary comparison with experimental NPA output data.

Two drift velocity distributions are especially expedient: (1) v_c independent of r_c/r_D and (2) v_c proportional to r_c/r_D. Case 1 may be argued to apply, for example, when the bulk of the plasma is outside of sheath regions and the applied E field is dominant. If a field induced by ambipolar diffusion, however, were dominant, then

$$E = (kT_e/en_i)dn_i/dr_c \tag{7}$$

(ref. 1). Use of a typical diffusion profile

$$n_i = n_i(0)e^{-(r_c/r_D)^2} \tag{8}$$

in equation (7) yields a result favorable to Case 2.

Simulation of the applied E field by that formed with a line source of electrons on the axis suggests that drift varies as $1/r_c$. Preliminary estimates, however, with use of this assumption did not yield good approximation to profiles obtained experimentally by verticle scans across the plasma.

For nonuniform drift the cyclotron radius must be less than some characteristic length over which the electric field undergoes appreciable change in order for the orbits, relative to v_c, to be approximated by circles.

Uniform Drift Velocity

For constant T_{cy} the integration of equation (6) over r_c/r_D is now dependent only on n_i and n_n. For an exponential density profile of neutrals as

$$n_n = n_n(0)e^{b_n(r_c/r_D)^2} \tag{9}$$

and a density profile for ions as in equation (8) it follows that

$$\frac{d\dot{N}_i}{d\mathscr{E}} = C\mathscr{A}\mathscr{H}\mathscr{K}n_i(0)n_n(0)\mathscr{E}\sigma_{ch}/2(1 - b_n) \int_{\theta_1}^{\theta_2} (1 + V_c \sin\theta/\sqrt{\mathscr{E}})$$

$$\times \exp -(\mathscr{E} + V_c^2 + 2V_c\sqrt{\mathscr{E}} \sin\theta)$$

$$\times \left\{ \exp\left[-(1 - b_n)(r_{c,1}/r_D)^2\right] - \exp\left[-(1 - b_n)(r_{c,2}/r_D)^2\right] \right\} d\theta \qquad (10)$$

where from equation (2)

$$\frac{r_{c,1}}{r_D} = \left[\frac{y}{r_D} \mp \mu(\sqrt{\mathscr{E}} + V_c \sin\theta)\right] \Big/ \sin\theta \qquad (11)$$

and

$$\mu \equiv r_{cy}/(r_D V_{cy}) = \sqrt{2mkT_{cy}}/(Br_D e) \qquad (12)$$

To determine $r_{c,2}/r_D$ replace y_1, in equation (11) with y_1, plus aperture height, h. The parameter μ can be considered as a mean cyclotron radius divided by the diffusion radius.

The limits of integration on θ are symmetrical about the y axis. They can be found simply by observing where the contribution to the flux reduces to zero during a numerical integration of equation (1). Approximate limits can be first obtained by use of figure 2(a) to make this process more efficient.

Drift Proportional to Radial Distance to Guiding Center

For this E field, and constant T_{cy}, it follows that V_c is equal to $V_c(1)r_c/r_D$.* Here $V_c(1)$ is the value of V_c where $r_c = r_D$. Equation (2) then becomes

---

*In this case centrifugal force, and azimuthal current due to unequal azimuthal drifts of electrons and ions (ref. 2) can be included in v_c since v_c remains proportional to r_c. Solution of the force equation (ref. 3) for v_c

$$-mv_c^2/r_c = q(E + v_c B)$$

by completing the square gives

$$v_c = r_c\left[\pm \sqrt{(\omega_{ci}/2)^2 - qE(1)/m} - \omega_{c,i}/2\right] = r_c v_c(1)$$

$$(r_c \sin \theta)/r_D = (y/r_D \mp \mu\sqrt{\mathscr{E}})/[1 \pm \mu V_c(1)] \equiv Y \qquad (13)$$

Note that the boundaries of the guiding center regions are now straight lines parallel to the x axis. The flux equation can now be written as

$$\frac{d\dot{N}}{d\mathscr{E}} = \eta e^{\mathscr{E}} \int_{Y_1}^{Y_2} \frac{\mathscr{E} + V_c(1)\sqrt{\mathscr{E}}\, Y}{Y\left[\kappa + V_c^2(1)\right] \exp\{2[\mathscr{E} + V_c(1)\sqrt{\mathscr{E}}\, Y\}} \int_{\theta_1}^{\theta_2} \frac{\psi^2/\sin^2\theta}{\exp(\psi^2/\sin^2\theta)}\, d\theta\, dY \qquad (14)$$

where

$$\psi \equiv \sqrt{\kappa + V_c^2(1)}\; Y,$$

$$\kappa = 1 - b_n$$

and

$$\eta = C \cancel{\mathscr{P}}\sigma_{ch}n_i(0)n_n(0)$$

With the substitution $\xi = \psi/\tan\theta$, the integration over θ can be performed to yield

$$-\sqrt{\pi}\; \psi e^{-\psi^2}[\text{erf}(\psi \cot \theta_2) - \text{erf}(\psi \cot \theta_1)]/2$$

which is approximately equal to $-\sqrt{\pi}\; \psi/e^{\psi^2}$. The resulting final integral, over Y, can be simplified by transforming to integration over Z where

$$Z = \sqrt{\mathscr{E}}\; V_c(1)Y + \mathscr{E}V_c^2(1)/[\kappa + V_c^2(1)]$$

This gives the final result

$$\frac{d\dot{N}}{d\mathscr{E}} = -\frac{\sqrt{\pi\mathscr{E}}\; \eta}{2\mathscr{V}^{3/2}} \left\{ \frac{V_c(1)\left[\exp(-\mathscr{V}Y_1^2 - 2V_c(1)\sqrt{\mathscr{E}}\; Y_1) - \exp\left(-\mathscr{V}Y_2^2 - 2V_c(1)\sqrt{\mathscr{E}}\; Y_2\right)\right]}{\exp(\mathscr{E})} \right.$$

$$\left. + \kappa \sqrt{\frac{\pi\mathscr{E}}{\mathscr{V}}}\; \frac{\text{erf}\left[\sqrt{\frac{V_c^2(1)\mathscr{E}}{\mathscr{V}}} + \sqrt{\mathscr{V}}\; Y_2\right] - \text{erf}\left[\sqrt{\frac{V_c^2(1)\mathscr{E}}{\mathscr{V}}} + \sqrt{\mathscr{V}}\; Y_1\right]}{\exp(\mathscr{E}\kappa/\mathscr{V})} \right\} \qquad (15)$$

where

$$\mathscr{V} \equiv \kappa + V_c^2(1),$$

$$Y_1 \equiv (y_1/r_D \mp \mu \mathscr{E})/[1 \pm \mu V_c(1)] \tag{16}$$

and for Y_2 replace y_1 in equation (16) with $y_1 + h$.

Numerical Calculations

The expressions for $d\dot{N}/d\mathscr{E}$ (eq. (6), (10), and (15)) are dependent on the parameters T_{cy}, μ, $V_c(1)$, y_1/r_D, and h/r_D for ε set by the NPA. Selection of the radial distribution of V_c, n_i, and n_n must also be made. All curves will be normalized such that their peak values reach unity. Thus, the constants $n_i(0)$ and $n_n(0)$ of equations (8) and (9) do not influence results in the paper. The detector characteristic, $\mathscr{K}$, is assumed constant and $\mathscr{G}$ assumed proportional to ε. The energy distribution can then be calculated provided sufficient data are available to determine σ_{ch} and $\mathscr{F}$.

Curves were fitted to the charge exchange and fractional ionization data for the species of interest (figs. 3 and 4). When required, numerical integration was performed by use of Gaussian quadratures with an IBM 7094 digital computer.

COMPARISON OF THEORETICAL RESULTS WITH NPA OUTPUT

Theoretical results were compared with NPA output data from four crossed-field type plasma heating devices (refs. 4, 5, 6, and 7). Available from all of these investigations are curves of $d\dot{N}/d\varepsilon$ against ε for helium and/or various hydrogen species. In addition, traverses in the y direction of the diagnostics plane were made in the Lewis HIP and SUMMA plasma heating devices. Such vertical scans are most helpful in the study of radial density distributions. The energy traces, however, were quite insensitive to density distributions, but were of prime importance in the estimation of T_{cy} and v_c. Unless otherwise stated, uniform neutral ($b_n = 0$) and diffusion type ion (eq. (8)) density profiles were used in the numerical calculations presented for the energy distribution. Bending magnets were used on the NPA of references 4, 5, and 7 so that only particles having a specified mass-to-charge ratio could reach the detector.

Energy Distribution Parameters $\Delta\varepsilon$ and ε_p

The various energy distribution curves can be quite well identified by the combination of their half widths, $\Delta\varepsilon$, and their most probable energy, ε_p; that is, the energy at which the NPA output current is a maximum. Plots of $\Delta\varepsilon$ against ε_p enable an insight into the extent of influence of a number of variables on the energy distributions. Results for He^+ ions charge-exchanging on He neutrals, for a B field of 2 tesla, are shown in figures 5(a) and (b).

The difference of results obtained by use of the two azimuthal drift assumptions is very pronounced. Results based on case 1 (V_c independent of r_c) form a grid of widely separated lines of constant V_c, whereas results based on case 2 (V_c proportional to r_c) form such a narrow band that they can be represented as one straight line which is independent of B as well. For hydrogen this band is slightly curved and not quite so narrow.

Constant μ lines coincide with those of constant T_{cy}; see equation (12). Where μ increases beyond unity, the mean cyclotron radius is greater than the diffusion radius and use of a guiding center model becomes progressively less justifiable.

Values of $\Delta\varepsilon$ and ε_p obtained from NPA otuput traces on an x-y recorder are shown by the data points on figure 5(b). Two operating lines can be distinguished. One is for the cylindrical type anode used in both HIP and SUMMA; the other for a water-cooled ring anode used only in SUMMA. Both lines are to the right of the case 1 line and well into the region of case 2.

Drift velocity, v_c, is next identified with E/B to show lines of various E values for constant B in figure 5(b). Quite reasonable values of E and T_{cy} were found in the interpretation of NPA results by use of such plots as long as μ was less than unity. These variables are more descriptive than V_c and μ and will therefore be presented in the following discussion.

Vertical Scans

A typical curve of current from the NPA output detector against y/r_D is shown by the line comprised of short dashes in figure 6(a). This trace from HIP was obtained with the electrostatic plates (ref. 8) at a fixed energy setting of 3.5 keV. This is near ε_p for the test conditions which were 13.5 kilovolts across the electrodes and a 1.1 tesla B field.

Vertical scan results are shown for both the constant drift and the drift proportional to r_c theory even though this latter theory does not give energy distributions which agree with NPA data at high V_c (fig. 5(a)).

The shape of the energy distribution curve (not shown) was well approximated by assuming $T_{cy} = 0.65$ keV, $h/r_D = 1.6$, and a uniform E = 2700 V/cm. The visible radius of the plasma was approximately 2 centimeters in HIP, thus r_D was set at 1 centimeter. (With a diffusion profile approximately 98 percent of the plasma lies within $r_c/r_D = 2$.) Using these conditions, with the exception that $h/r_D = 0.8$, in the $V_c \propto r_c$ theory gave results which also agree quite well with the shape of (although vertically displaced from) the NPA trace. The absolute y/r_D location of the experimental curve is not

known within about 0.5 centimeter, so that only the shape and relative y/r_D location of the theoretical curves can be appraised. The theoretical curves have an asymmetry about their peaks which is not as apparent in the experimental curve. Figure 6(b) illustrates the sensitivity of the profile to h/r_D. Results for both E type of drift variations are insensitive to aperture height below an h/r_D of 0.2.

At high values of T_{cy} the density of neutrals should be considerably reduced at the center of the plasma. An arbitrary density distribution of neutrals using $b_n = 0.75$ was calculated in conjunction with the previous conditions. This profile has relatively few neutrals at the plasma axis (5 percent) compared to that at the outer edges (where $r/r_D = 2$) consistent with trends of references 9 and 10. The shape of the profile (fig. 5(a)) was quite insensitive to changes in b_n, but the peak of the curve shifted to higher y/r_D with increase of b_n. Location of the profile peak may thus be useful in determining neutral density profile.

Energy Distribution Curves

A closer determination of E and T_{cy} values from the NPA traces, than those obtained from $\Delta\varepsilon$ and ε_{mp} values, can be made by comparing entire curves. Figures such as 5(a), however, provide excellent starting points from which the E and T_{cy} values can be adjusted for better curve fits.

Figure 7(a) shows a family of curves obtained from SUMMA operating with helium. The B field was varied from 1.1 to 3.3 tesla while the voltage (across a cathode-anode combination at each end of the plasma) was held constant at 5 kilovolts. The theoretical lines were obtained using the uniform drift theory with $h/r_D = 1.6$. Note that the whole family of NPA traces can be quite well matched with consistent guiding center model curves.

Plots of E, V_c, μ, and T_{cy} values, determined by the theory, against B is shown in figure 8. Results indicate that increasing B enables maintenance of higher radial E fields in the measuring plane midway between the two sets of electrodes. Increasing B reduces the drift energy. Since drift energy is in part transferred into random energy it is quite plausible that T_{cy} should decrease with increase of B. At low B values but at higher voltages it was found that V_c can be considerably less than one. Thus the drift energy can be much less than the random energy indicating contributions also from another mechanism, such as resistive and/or turbulent heating.

Applications of the guiding model to data obtained from the Lewis Bumpy Torus operating with deuterium is shown in figure 9. The data presented here, although nontypical of this device, were selected since B and T_{cy} are especially low causing V_c to be very high. Theory predicts that the separation between the ε_p of different mass-charge

ratio species increases with increase of V_c.

The curves of both D^+ and D_2^+ were quite well fitted with
$E = 1$ kV/cm and $T_{cy} = 100$ eV in the theory. Relatively flat ion
density profiles ($n_i = n_i(0)e^{-r_c/r_D}$) were used, guided by the results
in reference 6 for the high current mode.

Data from the Oak Ridge Burnout V apparatus are shown in figure 10
for atomic hydrogen (ref. 7). It is quite significant that the value
of ion temperature reported in this reference is very close to the value
($T_{cy} = 1.25$ keV) giving the best guiding center model agreement with the
NPA data. An E field of 6.5 kV/cm was obtained from the theory. This
is reasonable for the 10 kV applied at the electrodes in the experiment.

CONCLUSIONS

The guiding center model offers explanation to a number of the domi-
nant features of NPA output traces obtained from crossed-field heating
devices which have a characteristic azimuthal drift. The half widths as
well as the most probable energy of the NPA energy distributions were
found to increase with temperature of the cyclotron component, with mass-
charge ratio of the ions, and with the strength of the radial electric
field. The separation of output peaks between two different mass-charge
species in the same plasma increases with the ratio of drift velocity to
mean cyclotron velocity. Of the two radial drift distributions studied,
the one independent of radial distance from the center of the plasma
yielded results which best fit the NPA data.

The guiding center model indicates that NPA energy distributions
are quite insensitive to radial density distributions of both ions and
neutral background particles. Vertical scans obtained in HIP and SUMMA
heating devices with the NPA energy selector held constant gave contours
of current against vertical displacement across the plasmas which agree
well with guiding center model results based on a diffusion density pro-
file for ions. Theory indicates a vertical shift of the curve peaks with
decrease of neutral density near the plasma axis of symmetry. Increase
of drift velocity causes a shift in the opposite direction.

APPENDIX – SYMBOLS

[The International System of Units is used unless otherwise stated.]

A   mass number

a   constant in definition of parallel velocity distribution function

B   magnetic flux density

b   constant in equation (9)

C   constant in equation (6)

E   electric field strength

$\mathcal{C}$ dimensionless energy, ε/kT_{cy}

$\mathcal{H}$ stripping cell efficiency

f   velocity distribution function

$\mathcal{Y}$ beam resolution

h   aperture height

$\mathcal{K}$ detector efficiency

k   Boltzmann constant

ℓ aperture length

m   mass

$\dot{N}$ number of particles per unit time

n   number density

q   charge

r   radius

T   temperature

V   dimensionless velocity

$\mathcal{V}$ $\kappa + v_c^2(1)$

v   velocity

x,y,z   Cartesian coordinate; x and y are in the diagnostics plane; z is parallel to the plasma axis

Y   defined by equation (13) or (16)

Z   space used in integration of equation (14)

α angle between $\vec{v}_\parallel$ and $\vec{v}_a$

β angle between cyclotron and guiding center radii

ε energy

η coefficient in equation (14)

θ angle between cyclotron radius and x axis

κ $1 - b_n$

μ ratio of mean cyclotron radius to diffusion radius

ξ $\psi / \tan \theta$

σ cross section

ϕ azimuthal angle about $\vec{B}$ in velocity space

ψ $\sqrt{\kappa + v_c^2(1)}\ Y$

ω cyclotron frequency

Subscripts:

a   aperture

c   guiding center

ch   charge exchange

cy   cyclotron

D   diffusion

e   electron

i   ion

n   neutral

p   most probable

v   velocity

$\parallel$ parallel

$\perp$ perpendicular

REFERENCES

1. Engel, A. von: Ionized Gases. Second ed., Oxford Clarendon Press, 1965, p. 247.

2. Hirose, A.; and Alexeff, I.: Electrostatic Instabilities Driven by Currents Perpendicular to an External Magnetic Field. Nucl. Fusion, vol. 12, no. 3, May 1972, pp. 315-323.

3. Artsimovich, Lev A.: Controlled Thermonuclear Reactions, Gordon and Breach Science Publishers, 1964, p. 337.

4. Sigman, Donald R.; and Reinmann, John J.: Steady State Hot-Ion Plasma Produced by Crossed Electric and Magnetic Fields. NASA TM X-2783, 1973.

5. Reinmann, J. J.; et al.: Hot Ion Plasma Heating Experiments in SUMMA. NASA TM X-71559, 1974.

6. Roth, J. Reece; Richardson, Richard W.; and Gerdin, Glenn A.: Initial Results from the NASA Lewis Bumpy Torus Experiment. NASA TM X-71468, 1973.

7. Stirling, W. L.: Lifetime of Hot-Ion Plasma in a Mirror Machine. Phys. Fluids, vol. 15, no. 4, Apr. 1972, pp. 688-692.

8. Valckx, F. P. G.: Electrostatic Analyzer for the Detection of Fast Neutral Particles. NASA TT F-11458, 1968.

9. Parsons, C. R.; and Medley, S. S.: On the Interpretation of Charge-Exchange Ion Temperature Measurements in Tokomaks. Plasma Phys., vol. 16, no. 3, Mar. 1974, pp. 267-273.

10. Konstantinov, O. V.; and Perel, V. I.: The Energy Distribution of Heat Neutral Atoms Issuing from a Plasma. Soviet Phys.-Tech. Phys., vol. 5, no. 12, June 1961, pp. 1403-1406.

11. Nagey, Stephen W.; Savola, William J., Jr.; and Pollack, Edward: Measurement of the Total Cross Section for Symmetric Charge Exchange in Helium from 400-2000 eV. Phys. Rev., vol. 177, no. 1, Jan. 5, 1969, pp. 71-76.

12. Shelton, W. N.; and Stoycheff, P. A.: Measurement of the Total Cross Section for Single-Electron Transfer in Collisions of He^+ with He in the Energy Range 2-22 keV. Phys. Rev. A, vol. 3, no. 2, Feb. 1971, pp. 613-619.

13. Allison, Samuel K.: Experimental Results on Charge-Changing Collisions of Hydrogen and Helium Atoms and Ions at Kinetic Energies above 0.2 keV. Rev. Mod. Phys., vol. 30, no. 4, Oct. 1958, pp. 1137-1168.

14. Fite, W. L.; Smith, A. C. H.; and Stebbings, R. F.: Charge Transfer in Collisions Involving Symmetric and Asymmetric Resonance. Proc. Roy Soc. (London), Ser. A, vol. 268, no. 1335, Aug. 1962, pp. 527-536.

15. Fite, Wade L.; Stebbings, R. F.; Hummer, David G.; and Brackmann, R. T.: Ionization and Charge Transfer in Proton-Hydrogen Atom Collisions. Phys. Rev., vol. 119, no. 2, July 15, 1960, pp. 663-668.

16. Cramer, W. H.: Elastic and Inelastic Scattering of Low-Velocity H^+ and H_2^+ in Hydrogen. J. Chem. Phys., vol. 35, no. 3, Sept. 1961, pp. 836-838.

17. Cramer, W. H. and Marcus, A. B.: Elastic and Inelastic Scattering of Low-Velocity D^+ and D_2^+ in Deuterium. J. Chem. Phys., vol. 32, no. 1, Jan. 1960, pp. 186-188.

18. McClure, G. W.: Charge Exchange and Dissociation of H^+, H_2^+, and H_3^+ Ions Incident on H_2 Gas. Phys. Rev., vol. 130, no. 5, June 1, 1963, pp. 1852-1859.

19. Schmid, Albert: Dissoziation und Umladung von Wasserstoff- and Deuterium-Molekülionen beim Durchgang durch Wasserstoff. Z. Physik, vol. 161, Feb. 1961, pp. 550-559.

20. Stier, P. M.; and Barnett, C. F.: Charge Exchange Cross Sections of Hydrogen Ions in Gases. Phys. Rev., vol. 103, no. 4, Aug. 15, 1956, pp. 896-907.

21. Barnett, C. F.; and Ray, J. A.: A Calibrated Neutral Atom Spectrometer for Measuring Plasma Ion Temperatures in the 0.165 to 10 keV Energy Region. Nucl. Fusion, vol. 12, no. 1, Jan. 1972, pp. 65-72.
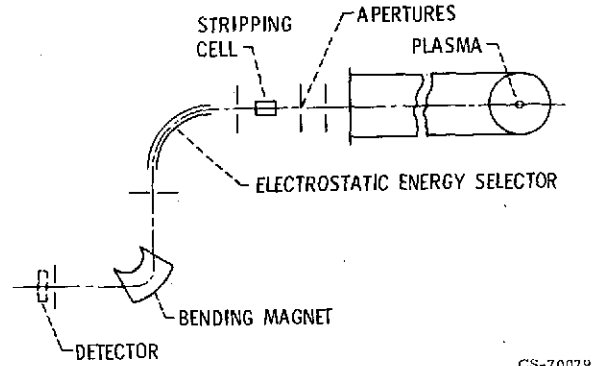
Figure 1. - Neutral particle analyzer.
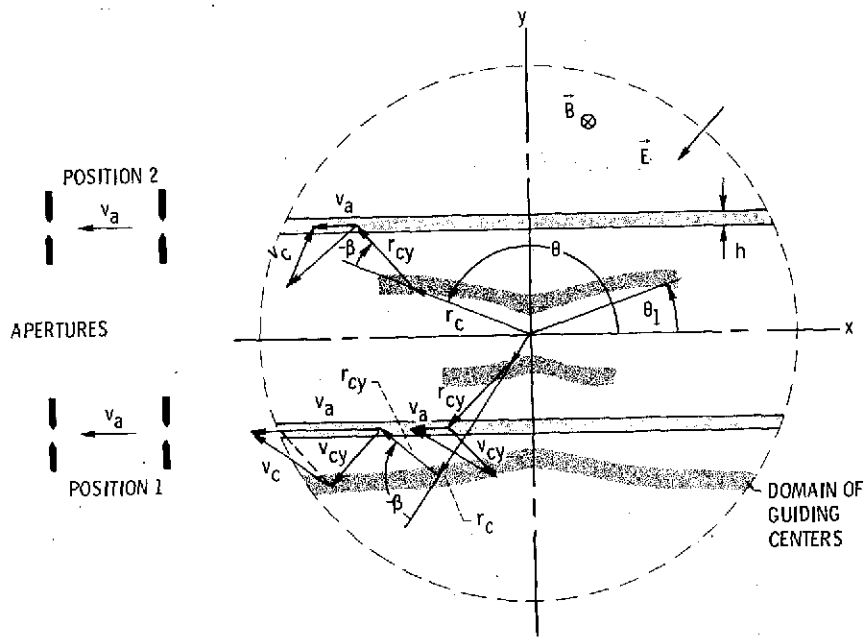
(a) NEUTRALS ENTERING APERTURES IN x, y PLANE NORMAL TO PLASMA AXIS. TWO VERTICAL POSITIONS OF THE APERTURES ARE SHOWN.

Figure 2. - Guiding center model vector diagrams.
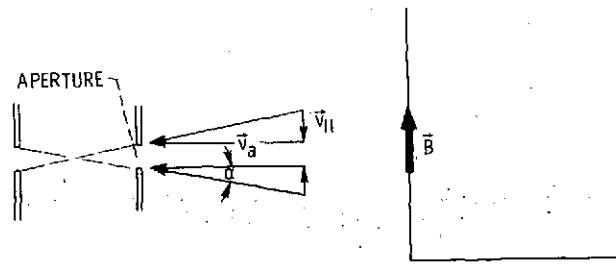
(b) NEUTRALS ENTERING APERTURES IN x, z PLANE PARALLEL TO PLASMA AXIS.
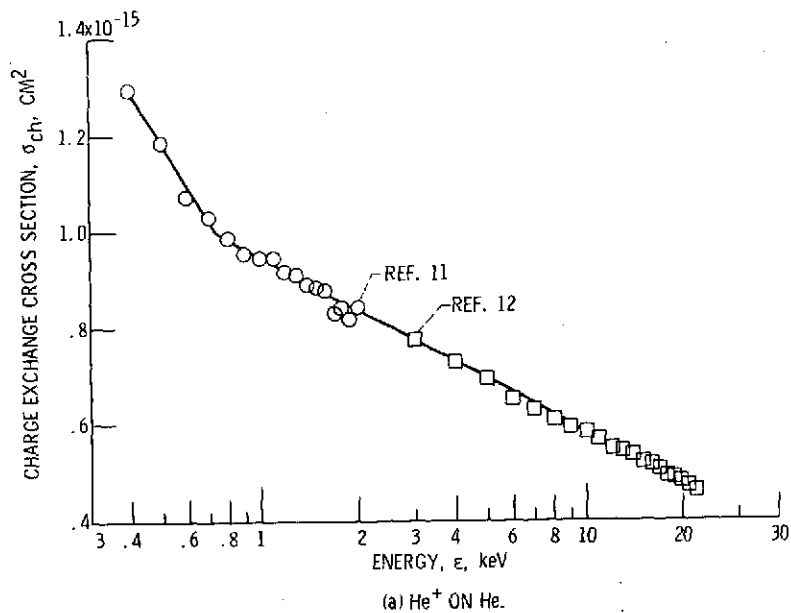
Figure 2. - Concluded.

Figure 3. - Charge exchange cross sections. Lines denote fit to data used in numerical calculations.
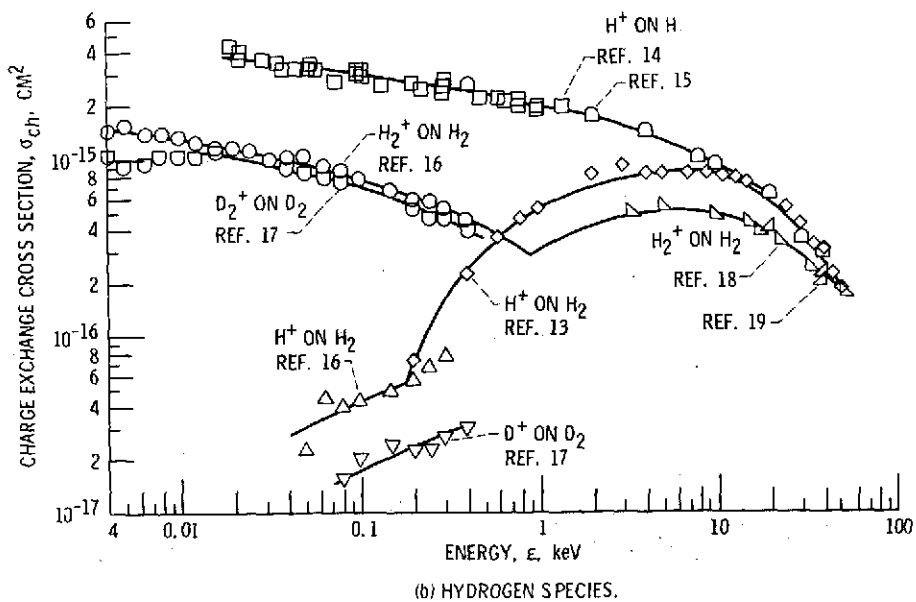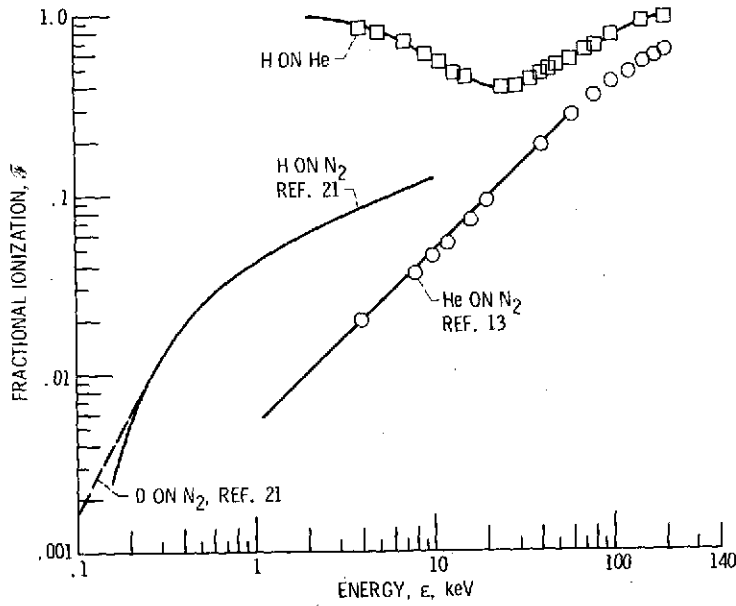
(a) He$^+$ ON He.

(b) HYDROGEN SPECIES.

Figure 3. - Concluded.

Figure 4. - Fractional ionization in stripping cell. Data of reference 21 extrapolated to 0.1 torr.
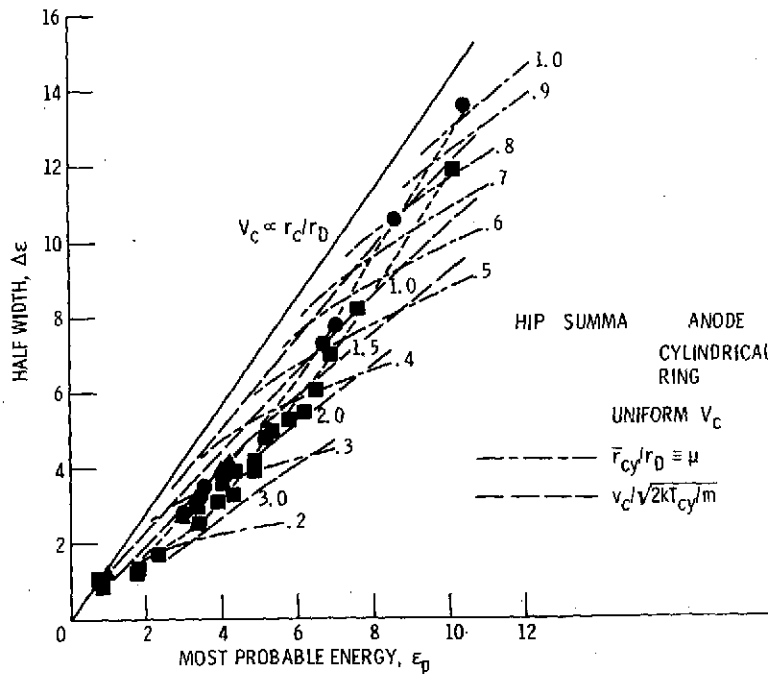
(a) USE OF V_c AND μ GRID LINES. EXPERIMENTAL DATA OBTAINED AT B FIELDS RANGING FROM 1.0 TO 3.5 TESLA.

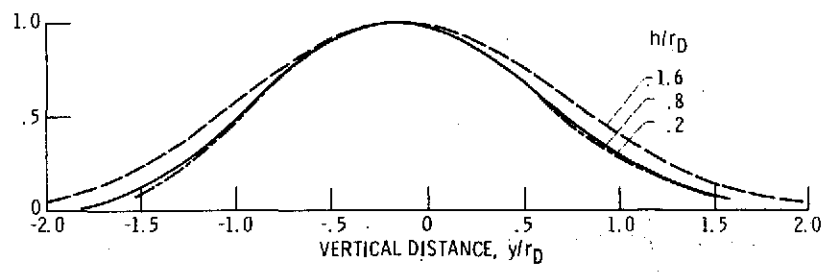Figure 5. - Uniform E performance grid for helium. B = 2 tesla, h/r_D = 1.6, b_n = 0.
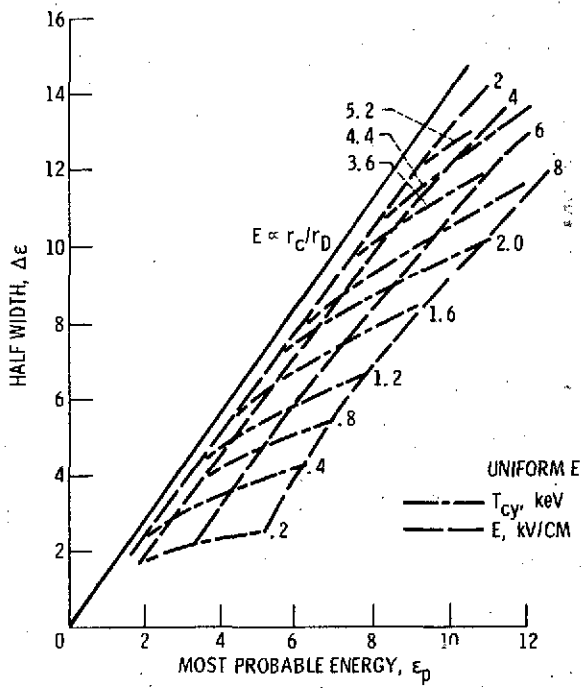
(b) USE OF E AND T_{cy} GRID LINES.

Figure 5. - Concluded.
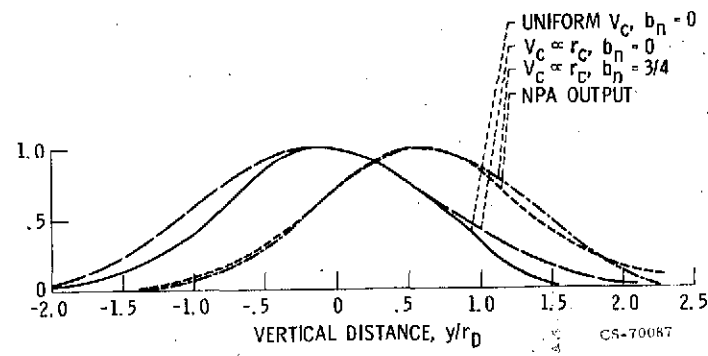
(a) $h/r_D = 1.6$.

Figure 6. - Comparison of theory with helium data from HIP. Anode voltage set at 13.5 kV. B = 1.1 tesla; E at $r_c/r_D = 1$ set at 2700 V/cm in theory; $T_{cy} = 0.65$ keV.

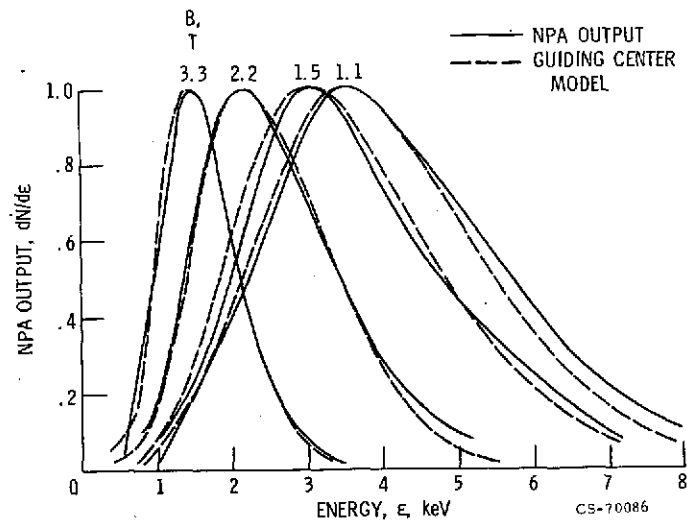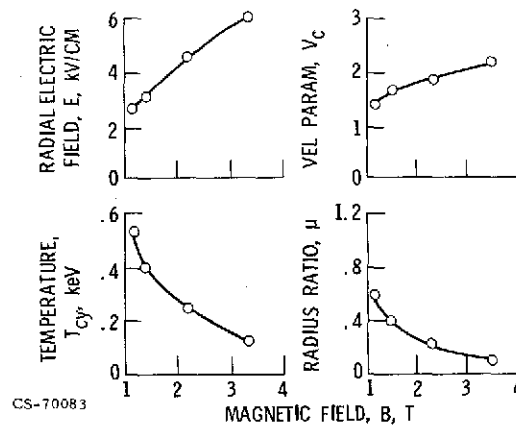(b) EFFECT OF APERTURE HEIGHT, $E \propto r_c/r_D$.

Figure 6. - Concluded.

Figure 7. - Comparison of uniform E theory with measurement in SUMMA using helium. Electrode voltage = 5 kV, $h/r_D = 1.6$.

Figure 8. - Results determined from guiding center model with curve fits shown in figure 7.

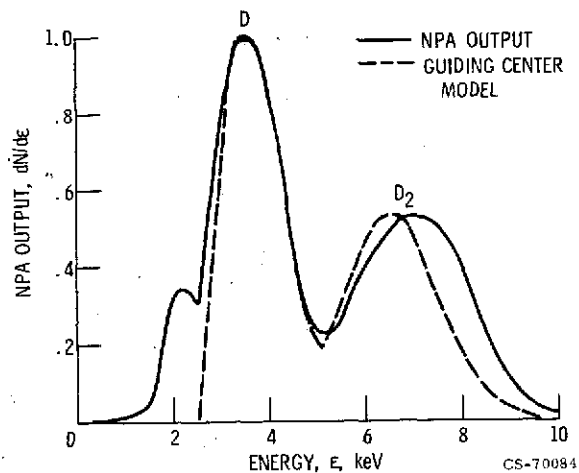Figure 9. - Comparison of theory with data from Lewis Bumpy Torus using deuterium. Anode voltage set at 5 kV. B = 0.2 tesla; $h/r_D = 0.14$; $n_i \propto \exp(r_c/r_D)$; $V_c/\sqrt{A} = 3.6$; $\mu/\sqrt{A} = 0.65$.

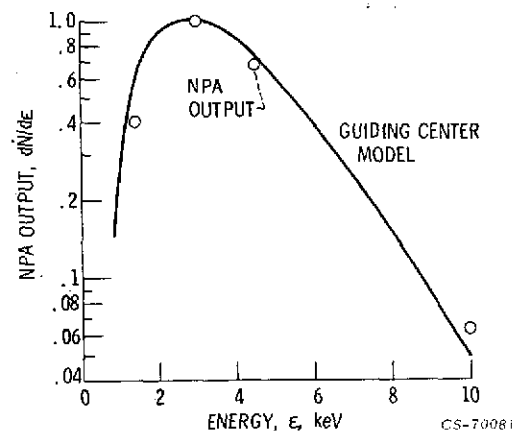Figure 10. - Comparison of theory with Oak Ridge Burnout V data for H^+ charge exchanging on H. B = 2.5 tesla; $h/r_D = 1$; uniform E = 5 kV/CM; $T_{cy} = 1$ keV.